# Entanglement from Tensor Networks on a Trapped-Ion Quantum Computer

Michael Foss-Feig,[1*] Stephen Ragole,[1] Andrew Potter,[2] Joan Dreiling,[1] Caroline Figgatt,[1] John Gaebler,[1] Alex Hall,[1] Steven Moses,[1] Juan Pino,[1] Ben Spaun,[1] Brian Neyenhuis,[1] and David Hayes[1]

[1]*Quantinuum, 303 South Technology Court, Broomfield, Colorado 80021, USA*

[2]*Department of Physics and Astronomy, and Quantum Matter Institute, University of British Columbia, Vancouver, British Columbia V6T 1Z1, Canada*

(Received 15 October 2021; accepted 25 March 2022; published 13 April 2022)

The ability to selectively measure, initialize, and reuse qubits during a quantum circuit enables a mapping of the spatial structure of certain tensor-network states onto the dynamics of quantum circuits, thereby achieving dramatic resource savings when simulating quantum systems with limited entanglement. We experimentally demonstrate a significant benefit of this approach to quantum simulation: the *entanglement structure* of an infinite system—specifically the half-chain entanglement spectrum—is conveniently encoded within a small register of "bond qubits" and can be extracted with relative ease. Using Honeywell's model H0 quantum computer equipped with selective midcircuit measurement and reset, we quantitatively determine the near-critical entanglement entropy of a correlated spin chain directly in the thermodynamic limit and show that its phase transition becomes quickly resolved upon expanding the bond-qubit register.

DOI: 10.1103/PhysRevLett.128.150504

Of the many applications considered for near-term quantum computers, the simulation of strongly correlated quantum systems stands out for being useful, hard classically, and tolerant of at least some imperfections (nature is, after all, a noisy place). Yet even in simulating quantum systems, a problem so well tailored to quantum computing that it is often credited with initiating the field, solving classically hard problems of real utility remains stubbornly out of reach. Part of the difficulty is that—unlike the outputs of random unitaries [1,2]—states of physical quantum systems are highly structured, which the best classical algorithms exploit; quantum advantage may well require quantum algorithms that can similarly exploit this structure. Notable recent progress has been made along these lines, with quantum algorithms designed around various classical tensor-network methods [3–11]. Here, we demonstrate for the first time a remarkable feature of these algorithms: in addition to inheriting considerable resource savings from their classical precursors, they also provide a remarkably direct encoding of the entanglement structure in states they represent. The latter point is especially enticing, as many-body entanglement entropy offers valuable information-theoretic insights into the structure of complex quantum matter that cannot be captured by local correlations [12,13]; understanding its structure sheds light on the quantum foundations of thermodynamic entropy [14], thermalization and quantum chaos [15], and even perhaps the geometry of space-time itself [16]. Moreover, universal scaling features of entanglement [17], such as central charge and its higher dimensional analogs, have entanglement-based interpretations and serve as fingerprints of critical phenomena.

A key technical challenge in running many such algorithms is the necessity to perform selective midcircuit measurement, reset, and reuse (MCMR) of qubits during a quantum circuit. Long recognized as a crucial ingredient for scalable quantum computation, this ability and other closely related capabilities have been realized in several quantum computing platforms [18–20]. Trapped ions in particular afford several convenient and high-fidelity approaches, including dynamic spatial isolation [18,21,22], shelving [23], and dual-species quantum logic gates [24–26]. Until very recently [27–29], however, MCMR had not been implemented on commercial quantum computing hardware.

In this Letter, we use a trapped-ion quantum computer equipped with MCMR [Fig. 1(a)] to implement an efficient quantum algorithm for extracting the near-critical entanglement entropy of correlated spin chains. We apply this algorithm to the transverse-field Ising model (TFIM) [30], and are able to clearly and quantitatively observe the divergence of bipartite entanglement entropy upon approaching the quantum phase transition separating its ordered and disordered phases.

In its simplest incarnation, the algorithm we employ involves one "system qubit," one "bond qubit," and repeated applications of the process shown in Fig. 1(b): (1) reset the system qubit, (2) apply a unitary entangling operation between the system qubit and bond qubit, and (3) measure the system qubit. More generally, an $n_b$-qubit bond register propagates spatial correlations of an arbitrary bond dimension $\chi = 2^{n_b}$ matrix product state (MPS)

 

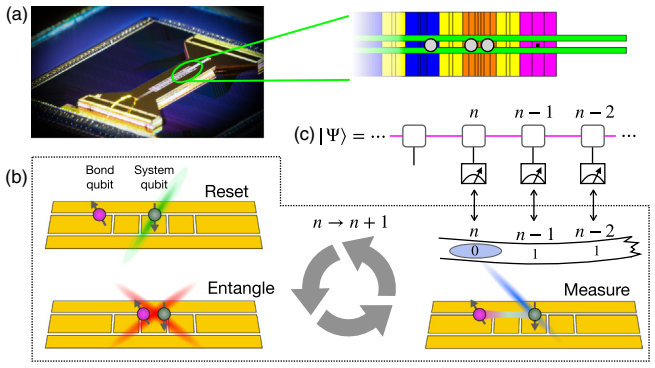


FIG. 1. Using Honeywell's H0 quantum computer described in Ref. [29] and shown in (a), we execute a state-preparation algorithm for arbitrary matrix-product states (MPS) (b). (c) The algorithm consists of repeatedly entangling a *single* system qubit (gray) with a register of $\log\chi$ "bond" qubits (purple) in order to encode a bond dimension $\chi$ MPS (here we show the case of $\chi = 2$, which requires a single bond qubit). The spatial extent of the MPS is encoded in the temporal extent of the algorithm, with properties of the $n$th site corresponding to the measurement record of the system qubit prior to reset at the $n$th iteration.

through time, and each successive (in time) measurement of the system qubit extracts local information about the next adjacent site in the spatial extent of the MPS [Fig. 1(c)], from which we reconstruct an experimental estimate of its energy. Moreover, the reduced density matrix of the bond qubit after the $j$th iteration encodes the reduced density matrix of the half-chain containing sites up to and including $j$. The number of bond qubits $n_b$ determines the accessible MPS bond dimension $\chi$, which grows exponentially as $\chi = 2^{n_b}$, enabling an extremely rapid convergence of results in the number of available bond qubits. Our data show that even for $n_b = 2$ the divergence of entanglement entropy at the phase transition is quite sharply resolvable.

*Quantum MPS.*—Matrix product states are an ansatz designed to efficiently capture the properties of 1D systems with limited entanglement [31], and have been employed extensively in classical simulations of 1D and quasi-2D quantum systems [32]. An MPS of a half-infinite system with translationally invariant tensors [33] can be written

$$|\Psi\rangle = \sum_{\sigma_1,\alpha_1,\ldots} L^{\alpha_1}(V^{\alpha_1\alpha_2}_{\sigma_1} V^{\alpha_2\alpha_3}_{\sigma_2}\cdots)|\sigma_1,\sigma_2,\ldots\rangle. \quad (1)$$

Here, $\sigma_j$ indexes a set of basis states on site $j$, the $V^{\alpha\beta}_{\sigma}$ are tensors with bond indices $\alpha,\beta \in \{1,2,\ldots,\chi\}$ (with $\chi$ being the bond dimension of the MPS), and $L$ is a vector determining the left-boundary conditions. We restrict our attention to qubits as the physical degrees of freedom, in which case the physical indices take values $\sigma_j = 0, 1$ [34]. The MPS can be drawn schematically as in Fig. 2(a), where each tensor is a box with a leg for each index, and joined legs imply tensor contraction of the associated indices. Any MPS can be generated as a quantum circuit by

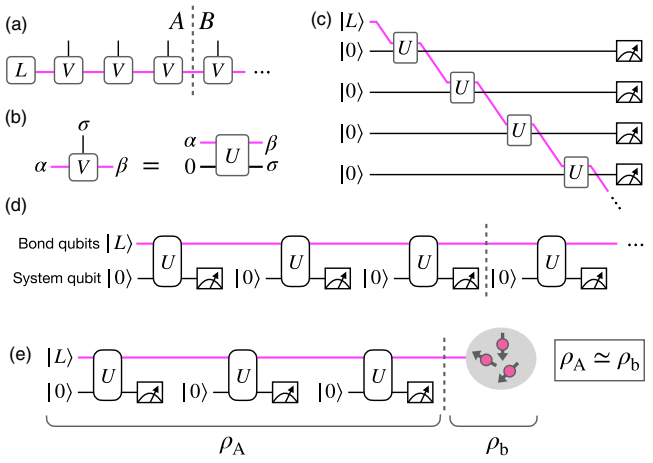


FIG. 2. Quantum MPS. The tensors of a matrix product state (a) can be embedded in unitary matrices (b) in order to generate the MPS as the output of a quantum circuit (c). By executing any desired measurements as soon as possible, the system qubit representing site $n$ can be reset and reused as the system qubit on site $n+1$, leading to an equivalent circuit with just a single system qubit (d). Entanglement entropy of the MPS across a bipartition (dashed vertical line in the figures) becomes entanglement entropy of the bond qubits immediately after crossing that partition (e), as future gates cannot affect the state prior to the partition.

embedding the tensors [35] in unitary matrices $U$ as $V^{\alpha\beta}_{\sigma} = (\langle\sigma| \otimes \langle\beta|)U(|0\rangle \otimes |\alpha\rangle)$ [see Fig. 2(b)], in which case the generating circuit involves a bond register interacting sequentially with the system qubits one by one,

$$|\Psi\rangle = \cdots U_{2,b}U_{1,b}(\cdots \otimes |0\rangle_2 \otimes |0\rangle_1) \otimes |L\rangle_b, \quad (2)$$

as shown in Fig. 2(c). As pointed out in Refs. [4–6], the sequential structure of the circuit in Fig. 2(c) enables any qubit to be sampled at the circuit output prior to the next qubit being gated, and therefore the entire circuit output can be sampled by repeatedly measuring, resetting, and reusing a single system qubit, as in Fig. 2(d).

Any MPS is equivalent to a quantum channel defined on the bond indices, which get reinterpreted as labeling states in a fictitious bond Hilbert space [36]. In the method just described for generating an MPS with one system qubit, the bond Hilbert space is explicitly realized by the bond-qubit register, and the process of initializing the system qubit, gating it with the bond qubit register, and then ignoring it (tracing it out) is precisely the unitary embedding (Stinespring dilation) of this bond-space quantum channel. A convenient consequence of this equivalence is that the bipartite entanglement spectrum induced by cutting an infinite chain into two halves $A$ and $B$, i.e., the eigenvalues of $\rho_A = \mathrm{Tr}_B(|\Psi\rangle\langle\Psi|)$, can be extracted from the steady state of this quantum channel [37]. The relationship between the entanglement spectrum of an MPS and the steady state of its associated channel is readily apparent in

the unitary embedding employed here. The infinite MPS case is well approximated by the half-infinite MPS we generate if we place the cut sufficiently far from the left boundary and then trace out the right (or left) half, as in Fig. 2(a). Figure 2(d) shows the state preparation scheme used here with the equivalent cut. Because the left half of the chain is fully formed immediately after the bond qubits reach the point in the circuit corresponding to the bipartition (dashed line), its entanglement entropy can only result from entanglement between it and the bond qubits, and can be extracted at that point without ever building the right half of the state. By the symmetry of entanglement spectra across the cut, the spectra of $\rho_A$ is then identical to that of the bond-qubit register at this point, as shown in Fig. 2(e).

*Demonstration*.—As an example of the MPS preparation technique and entanglement entropy extraction, we use Honeywell's model H0 QCCD trapped-ion quantum computer [29] to construct MPS approximations to the ground state of the transverse-field Ising model (TFIM), with Hamiltonian

$$H = -\sum_j (Z_j Z_{j+1} + \lambda X_j). \tag{3}$$

For transverse-field strengths $\lambda > 1$ the TFIM ground state is disordered with respect to the $\mathbb{Z}_2$ symmetry of the Hamiltonian, while for $\lambda < 1$ the ground state spontaneously breaks that symmetry, and these phases are separated by a continuous quantum phase transition. When approaching the transition from either side, the entanglement entropy diverges logarithmically [38], reflecting the divergent correlation length and serving as a sensitive probe of the phase transition [39].

The quantum computer operates with up to six qubits and two gate zones (see Ref. [29] for a detailed description of the quantum computer architecture and operations). Each qubit is encoded in the states $|1(0)\rangle \equiv |F = 1(0), m_F = 0\rangle$ of the $S_{1/2}$ ground-state hyperfine manifold of a $^{171}Yb^+$ ion, with $F$ and $m_F$ quantum numbers of the total internal angular momentum and its projection along a ≈5 G applied magnetic field, respectively. Qubit ions are cotrapped with an equal number of $^{138}Ba^+$ ions, which are used to sympathetically cool the motion of the qubits during a quantum circuit without impacting their logical state. All laser-based operations (gates, measurement, and reset) are carried out in the two gate zones shaded blue and orange in Fig. 1(a). The ions are stored in either Ba-Yb or Ba-Yb-Yb-Ba crystals, with single-qubit gates (average fidelity ≈99.97%) performed on the former and two-qubit gates (average fidelity ≈99.2%) on the latter. Arbitrary connectivity of two-qubit gates is achieved by physically rearranging the qubits between the various crystals into suitable pairs prior to gating the pairs within each crystal.

For the present demonstration, it is crucial that the system qubit can be selectively measured and reset in the middle of a circuit without impacting the bond qubits, which encode the MPS and its entanglement structure. Both reset and measurement involve applying resonant light either on a cycling transition (measurement) or to optically pump $|1\rangle \to |0\rangle$ (reset) [40], and even a single resonant photon scattered by a bond qubit causes an error on that qubit. To avoid such crosstalk, qubits that are measured or reset in the middle of a circuit are temporarily isolated [18,21,22] from all other qubits by at least 110 $\mu$m during the reset process, whereas the reset beams have an effective $1/e^2$ radius of ≈25 $\mu$m. MCMR crosstalk is further suppressed by using independent electrode control to push unmeasured qubits off the trap axis, inducing micromotion due to the rf trapping potential. This motion effectively causes the measurement and reset laser to appear phase modulated in the frame of the unmeasured qubits, displacing a large fraction of the already low laser intensity into off-resonant sidebands. Detailed analysis of the measurement and reset crosstalk in this system can be found in Ref. [41], but for our purposes it suffices to know that the average infidelity induced on spectator qubits due to reset (measurement) crosstalk is $\lesssim 4 \times 10^{-4} (2 \times 10^{-3})$.

In order to demonstrate the state preparation method and the extraction of entanglement entropy, we classically optimize MPS approximations to the TFIM ground state over a range of $\lambda$ and decompose their unitary embeddings into our native gate set. In principle, scaling these techniques to bond dimensions outside the reach of classical MPS optimization should be possible by utilizing parametrized circuits and feeding energy estimates from the quantum computer into a classical optimization routine [6,42]. We first perform a scan across the phase transition for a $\chi = 2$ MPS, which requires only a single bond qubit. Since the quantum computer has two gate zones we generally run 2 parallel copies of the state preparation scheme. While our goal is to extract entanglement entropy from the bond-qubit register, preparation of the bond qubit steady state by MPS channel iteration automatically provides an opportunity to sample local correlation functions along the way (after sufficient channel iterations to converge to bulk values, but prior to destructive measurement of the bond-qubit register). Utilizing identical circuits to those run for entanglement entropy measurements at bond dimension $\chi = 2$, we make sequential measurements of the system qubit in subsequent bases $X$, $Z$, $Z$, as shown in Fig. 3(a). For $j - 1$ iterations of the circuit block shown in the black-dashed box in Fig. 3(a), this procedure provides sufficient data to estimate both $\langle X_j \rangle$ and $\langle Z_{j+1} Z_{j+2} \rangle$, which (by discrete translational invariance) allows us to reconstruct $\langle H \rangle$ for large enough $j$. In practice, we always choose $j$ sufficiently large that boundary-induced errors are well below anticipated shot noise [43]. The results of these energy estimates for 5000 total shots per value of $\lambda$ are shown in Fig. 3(b), and are in good agreement with the exact ground-state energy of the infinite TFIM.

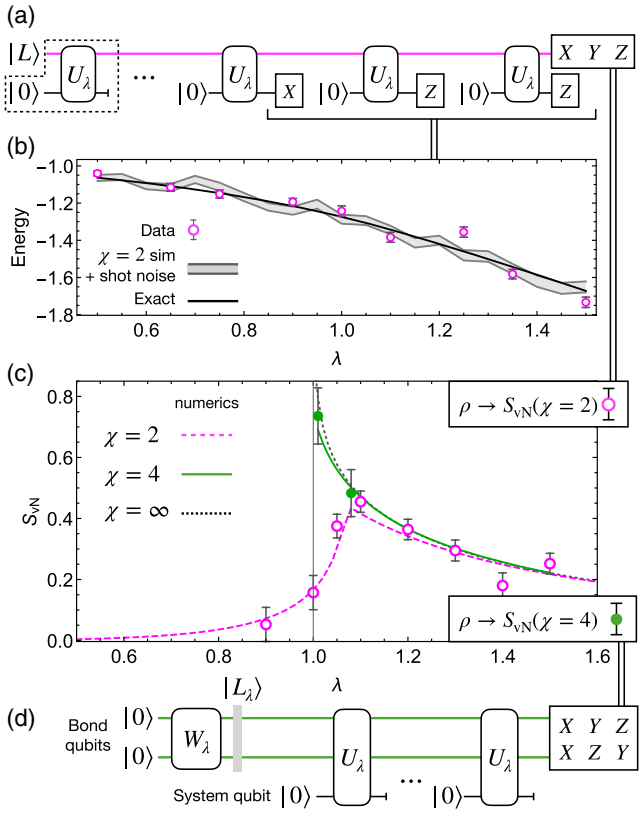


FIG. 3. (a),(b) Circuits for extracting bipartite entanglement entropy of a $\chi = 2$ (a) or $\chi = 4$ (b) MPS. (c) Measured entanglement entropy for the TFIM. Open purple circles are data taken with $n_b = 1$, and the purple dashed line shows the entanglement entropy of the lowest-energy MPS at $\chi = 2^{n_b} = 2$. Results using $n_b = 2$ are shown as filled green circles, and the solid green line corresponds to the lowest-energy $\chi = 4$ MPS. The black-dotted line is the exact entanglement entropy computed following Ref. [46]. All error bars represent $\pm\sigma$ confidence intervals obtained by bootstrapping. (a) Circuits to extract energy estimates from a bond dimension 2 MPS. (b) Solid line is the exact ground-state energy of the infinite-size TFIM. Experimental data (purple, $1\sigma$ error bars) agrees reasonably well from deep inside the ordered phase into the disordered phase. The gray shaded region is a $1\sigma$ confidence interval from a numerical simulation with the same shot-count as the experiment.

We extract the TFIM bipartite entanglement entropy by running the same circuits, except instead of making measurements on the system qubit [47] we simply extract the bond-register density matrix $\rho_b$ by state tomography after the $j$th iteration. Results for the entanglement entropy $S_{\mathrm{vN}} = -\mathrm{Tr}(\rho_b \log_2 \rho_b)$ are shown as open purple circles in Fig. 3(c), and agree well with numerical calculations of the bipartite entanglement entropy for the $\chi = 2$ MPS approximation to the ground state. At any finite bond dimension the peak entropy will also be finite, but the $\chi = 2$ peak is also significantly shifted toward the disordered side. This behavior is expected and reflects the tendency for any ansatz that limits entanglement (e.g., mean-field theory) to overestimate a system's inclination to order. To better resolve the entropy divergence at the critical point, we took more data just on the disordered side of the transition using one additional bond qubit, giving a $\chi = 4$ MPS [circuits shown in Fig. 3(d), data shown as filled green circles in Fig. 3(c)], and we see that the growth of entanglement near the true critical point becomes rapidly resolvable upon increasing the size of the bond qubit register. For comparison, a similarly accurate estimate of the entanglement entropy at the point nearest to the phase transition ($\lambda = 1.01$), if achieved by directly preparing the ground state of a large enough system to sufficiently suppress boundary effects, would require 40 qubits.

Note that all of the data in Fig. 3 utilize zero-noise extrapolation [44] to mitigate errors on the two-qubit gates [43]. For the $\chi = 4$ data, we also employ a symmetry-based selection criterion to reduce the number of measurement settings required for tomography of the bond-qubit register. While boundary effects can be suppressed arbitrarily by iterating the MPS channel a larger number of times, this comes at the cost of total run-time. To minimize run-time for the $\chi = 4$ circuits, we let the initial state of the bond-qubit register $|L_\lambda\rangle = W_\lambda|0\rangle \otimes |0\rangle$ be a function of $\lambda$, and classically optimized the unitary $W_\lambda$ to minimize the required burn in [43]. Note that this optimization always leaves the bond qubit in a pure state, so any measured entropy is due entirely to the application of the MPS channel itself. While the optimization of $W_\lambda$ was performed classically, we emphasize that it is not strictly necessary and was only performed to reduce run times (by about a factor of 3 at $\lambda = 1.01$ and less further from the transition). Moreover, this optimization could in principle be performed directly on the quantum computer at large bond dimension using a variational approach [9]. While the $\chi = 4$ results could in principle be continued across the phase transition into the ordered phase, the optimal circuits in the ordered phase are considerably more complex than in the disordered phase, leading to longer circuit run times and likely invalidating the application of our noise mitigation techniques.

*Outlook.*—Going forward it would be interesting to combine quantum tensor network algorithms with qubit-efficient schemes to measure Rényi entropies [48] in order to access larger bond-dimension MPS. Ultimately it is desirable to extend the present techniques to treelike or 2D tensor networks, and to quantum analogs of MPS time-evolution algorithms [6]; in both cases, large entanglement entropies often impede classical tensor-network-based simulations in practice, and quantum implementations with more than 30 qubits may provide a significant advantage [9,11,49,50].

We thank Karl Mayer for helpful discussions. This work was made possible by a large group of people, and the authors would like to thank the entire Quantinuum team for their many contributions. A. P. was supported by NSF Convergence Accelerator Track C Grant No. OIA 2040549.

*michael.feig@quantinuum.com


[1] F. Arute *et al.*, Nature (London) **574**, 505 (2019).
[2] H.-S. Zhong *et al.*, Science **370**, 1460 (2020).
[3] I. H. Kim, arXiv:1702.02093.
[4] W. Huggins, P. Patil, B. Mitchell, K. B. Whaley, and E. M. Stoudenmire, Quantum Sci. Technol. **4**, 024001 (2019).
[5] J.-G. Liu, Y.-H. Zhang, Y. Wan, and L. Wang, Phys. Rev. Research **1**, 023025 (2019).
[6] M. Foss-Feig, D. Hayes, J. M. Dreiling, C. Figgatt, J. P. Gaebler, S. A. Moses, J. M. Pino, and A. C. Potter, Phys. Rev. Research **3**, 033002 (2021).
[7] A. Smith, B. Jobst, A. G. Green, and F. Pollmann, arXiv:1910.05351.
[8] S.-H. Lin, R. Dilip, A. G. Green, A. Smith, and F. Pollmann, PRX Quantum **2**, 010342 (2021).
[9] F. Barratt, J. Dborin, M. Bal, V. Stojevic, F. Pollmann, and A. G. Green, npj Quantum Inf. **7**, 79 (2021).
[10] X. Yuan, J. Sun, J. Liu, Q. Zhao, and Y. Zhou, Phys. Rev. Lett. **127**, 040501 (2021).
[11] I. H. Kim and B. Swingle, arXiv:1711.07500.
[12] A. Kitaev and J. Preskill, Phys. Rev. Lett. **96**, 110404 (2006).
[13] M. Levin and X.-G. Wen, Phys. Rev. Lett. **96**, 110405 (2006).
[14] L. D'Alessio, Y. Kafri, A. Polkovnikov, and M. Rigol, Adv. Phys. **65**, 239 (2016).
[15] D. A. Abanin, E. Altman, I. Bloch, and M. Serbyn, Rev. Mod. Phys. **91**, 021001 (2019).
[16] T. Nishioka, Rev. Mod. Phys. **90**, 035007 (2018).
[17] P. Calabrese and J. Cardy, J. Stat. Mech. (2004) P06002.
[18] M. D. Barrett, J. Chiaverini, T. Schaetz, J. Britton, W. M. Itano, J. D. Jost, E. Knill, C. Langer, D. Leibfried, R. Ozeri, and D. J. Wineland, Nature (London) **429**, 737 (2004).
[19] W. Pfaff, T. H. Taminiau, L. Robledo, H. Bernien, M. Markham, D. J. Twitchen, and R. Hanson, Nat. Phys. **9**, 29 (2013).
[20] D. Ristè, M. Dukalski, C. A. Watson, G. de Lange, M. J. Tiggelman, Y. M. Blanter, K. W. Lehnert, R. N. Schouten, and L. DiCarlo, Nature (London) **502**, 350 (2013).
[21] J. Chiaverini, D. Leibfried, T. Schaetz, M. D. Barrett, R. B. Blakestad, J. Britton, W. M. Itano, J. D. Jost, E. Knill, C. Langer, R. Ozeri, and D. J. Wineland, Nature (London) **432**, 602 (2004).
[22] Y. Wan, D. Kienzler, S. D. Erickson, K. H. Mayer, T. R. Tan, J. J. Wu, H. M. Vasconcelos, S. Glancy, E. Knill, D. J. Wineland, A. C. Wilson, and D. Leibfried, Science **364**, 875 (2019).
[23] T. Monz, D. Nigg, E. A. Martinez, M. F. Brandl, P. Schindler, R. Rines, S. X. Wang, I. L. Chuang, and R. Blatt, Science **351**, 1068 (2016).
[24] P. O. Schmidt, T. Rosenband, C. Langer, W. M. Itano, J. C. Bergquist, and D. J. Wineland, Science **309**, 749 (2005).
[25] T. Rosenband, D. B. Hume, P. O. Schmidt, C. W. Chou, A. Brusch, L. Lorini, W. H. Oskay, R. E. Drullinger, T. M. Fortier, J. E. Stalnaker, S. A. Diddams, W. C. Swann, N. R. Newbury, W. M. Itano, D. J. Wineland, and J. C. Bergquist, Science **319**, 1808 (2008).
[26] V. Negnevitsky, M. Marinelli, K. K. Mehta, H. Y. Lo, C. Flühmann, and J. P. Home, Nature (London) **563**, 527 (2018).
[27] A. D. Corcoles, M. Takita, K. Inoue, S. Lekuch, Z. K. Minev, J. M. Chow, and J. M. Gambetta, Phys. Rev. Lett. **127**, 100501 (2021).
[28] Z. Chen, K. J. Satzinger, J. Atalaya, A. N. Korotkov, A. Dunsworth, D. Sank, C. Quintana, M. McEwen, R. Barends, P. V. Klimov *et al.*, arXiv:2102.06132.
[29] J. M. Pino, J. M. Dreiling, C. Figgatt, J. P. Gaebler, S. A. Moses, M. S. Allman, C. H. Baldwin, M. Foss-Feig, D. Hayes, K. Mayer, C. Ryan-Anderson, and B. Neyenhuis, Nature (London) **592**, 209 (2021).
[30] We chose the TFIM because it is simple and has well-understood critical properties, but the algorithm we describe is not restricted to integrable models, nor is it restricted to 1D [6].
[31] While many aspects of the discussion below generalize to more expressive tensor networks, including tree-tensor networks, MERA, and 2D isometric tensor networks, the key ideas are already contained in the simplest case of MPS, which are the focus of this demonstration.
[32] U. Schollwöck, Ann. Phys. (Amsterdam) **326**, 96 (2011).
[33] Translational invariance of the tensors leads to states that are asymptotically translationally invariant far from the left boundary.
[34] Systems with larger local dimension can also be simulated using qubits by associating more than one physical qubit to a lattice site.
[35] Such an embedding is ensured for any isometric tensor network, and any MPS can be made isometric by putting it in a suitable canonical form [32].
[36] N. Schuch, D. Pérez-García, and I. Cirac, Phys. Rev. B **84**, 165139 (2011).
[37] S. Gopalakrishnan and A. Lamacraft, Phys. Rev. B **100**, 064309 (2019).
[38] P. Calabrese and J. Cardy, Int. J. Quantum. Inform. **04**, 429 (2006).
[39] L. Tagliacozzo, T. R. de Oliveira, S. Iblisdir, and J. I. Latorre, Phys. Rev. B **78**, 024410 (2008).
[40] S. Olmschenk, K. C. Younge, D. L. Moehring, D. N. Matsukevich, P. Maunz, and C. Monroe, Phys. Rev. A **76**, 052314 (2007).
[41] J. Gaebler, C. Baldwin, S. Moses, J. Dreiling, C. Figgatt, M. Foss-Feig, D. Hayes, and J. Pino, Phys. Rev. A **104**, 062440 (2021).
[42] A. Peruzzo, J. McClean, P. Shadbolt, M.-H. Yung, X.-Q. Zhou, P. J. Love, A. Aspuru-Guzik, and J. L. O'Brien, Nat. Commun. **5**, 4213 (2014).
[43] See Supplemental Material at http://link.aps.org/supplemental/10.1103/PhysRevLett.128.150504 for details on unitary embeddings of MPS, boundary effects, error mitigations, and tomography protocols, which includes Refs. [44,45].
[44] K. Temme, S. Bravyi, and J. M. Gambetta, Phys. Rev. Lett. **119**, 180509 (2017).
[45] R. Stricker, D. Vodola, A. Erhard, L. Postler, M. Meth, M. Ringbauer, P. Schindler, T. Monz, M. Müller, and R. Blatt, Nature (London) **585**, 207 (2020).
[46] G. Vidal, J. I. Latorre, E. Rico, and A. Kitaev, Phys. Rev. Lett. **90**, 227902 (2003).
[47] In principle both energy and entanglement entropy can be measured in the same circuits, as intermediate measurement

of the system qubit does not affect the (marginalized) distribution of bond-qubit measurement outcomes. However, in order to minimize accumulated cross-talk errors we performed energy extraction and bond-qubit tomography on separate circuits.

[48] J. Yirka and Y. Subaşı, Quantum **5**, 535 (2021).

[49] R. Haghshenas, J. Gray, A. C. Potter, and G. K.-L. Chan, Phys. Rev. X **12**, 011047 (2022).

[50] E. Chertkov, J. Bohnet, D. Francois, J. Gaebler, D. Gresh, A. Hankin, K. Lee, R. Tobey, D. Hayes, B. Neyenhuis, R. Stutz, A. C. Potter, and M. Foss-Feig, arXiv:2105.09324.